Demultiplexing Spectrum-Sharing Field Sources with Distributed Field Probes

Daniel G. Kuester, *Member, IEEE*, Ryan T. Jacobs, Yao Ma, *Senior Member, IEEE*, and Jason B. Coder
U.S. Department of Commerce
National Institute of Standards and Technology
Communications Technology Laboratory, RF Technology Division
Boulder, Colorado 80305
Email: daniel.kuester@nist.gov, yao.ma@nist.gov, ryan.jacobs@nist.gov, jason.coder@nist.gov

***Abstract*—A complete characterization of multiple-device wireless interactions must include data relatable to the electromagnetic field radiated by each device under test (DUT). If these field sources are separable in time or frequency, they can be demultiplexed with a single probe antenna and time gating or bandpass filtering. Spectrum-sharing coexistence testing, however, may deal with simultaneous co-channel radiation. Communication channels may realize orthogonality in signal modulation or coding, for example, instead of time or frequency. These signals need an alternative to time or frequency as a basis to discriminate between signals in tests.**

We explore here distributed multi-probe detection as a means to address this problem. Simultaneous coherent detection of quadrature baseband at multiple probes provides degrees of freedom necessary to decompose modulated signals with different origins in space. The approximately deterministic simple propagation behavior in an anechoic chamber allows us to estimate channel delay, phase shift, and attenuation parameters between each combination of probes and DUTs. These parameters are sufficient to extrapolate a transfer matrix across frequency that we invert to compute a weighting matrix that deembeds the received superposition of DUT waveforms. We demonstrate experiments that demultiplex three DUTs: a 802.11n Wi-Fi link pair and a source of LTE traffic, all in overlapping channels near 2.4 GHz. The demultiplexed channels show clearly the channel occupancy of each DUT without time-gating or frequency filtering.

I. Introduction

Industry and government are developing technology, standards, and regulation policy to share spectrum allocations at the desirable frequencies below 6 GHz. The results of this work include the proposed Citizen's Broadband Radio Service (CBRS) near 3.5 GHz [1], IEEE 802.22 in TV whitespace bands [2], [3], and the well-known industrial, scientific, and medical (ISM) bands around 900 MHz, 2.4 GHz and 5.8 GHz. Increasing access to this spectrum presents an opportunity to increase wireless data network capacity if existing incumbent users can be protected from interference.

At its most basic, a spectrum sharing scheme needs to enable some type of separation of communication channels separable between different systems. Common mechanisms in ISM bands include frequency hopping and spread spectrum. Television whitespace use includes adaptive access by cognitive radio and a centralized database to minimize interference with regional television broadcasting. The proposed CBRS creates an elaborate three-tier sharing scheme built around a centralized spectrum access system (SAS) that coordinates use by non-government tiers [4]. Many approaches to adaptive spectrum access that use spectrum sensing may need to coexist, including combinations of physical orthogonality (time, frequency, space, or polarization) and/or signal orthogonality (like modulation or coding).

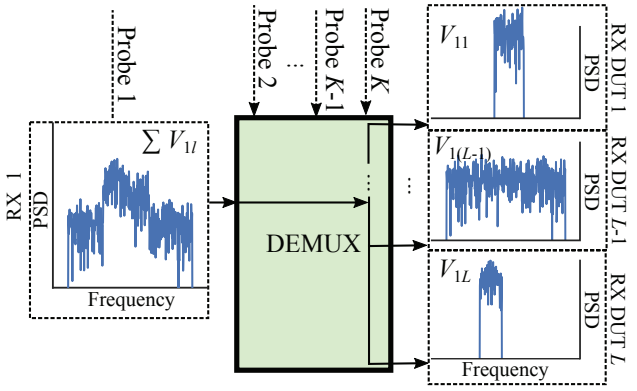

Fig. 1. Spatial demultiplexing ("DEMUX") decomposes a waveform received from multiple transmitter DUTs. The reference input waveform is defined at the reference port connected to probe 1. Coherent baseband receivers at probes 2 through K provide the additional necessary input degrees of freedom.

Spectrum-sensing and adaptive approaches like those above require tight coordination — ensuring proper radiation from each spectrum-sharing device becomes vitally important. Improper transmissions could be the result of product implementation errors, misconfiguration, or abuse, and may degrade communication network availability, data throughput, and latency. The modulation radiated by each transmitter is therefore exactly the fundamental quantity that needs to be captured to test coexistence. This means demultiplexing the signals superimposed over the air into separate channels, even when every radiator transmits different signals that are simulataneously in the same frequency band.

Current standards for over-the-air testing in the electromagnetic compatibility (EMC) and communication communities often approach measurements at the high and low extremes

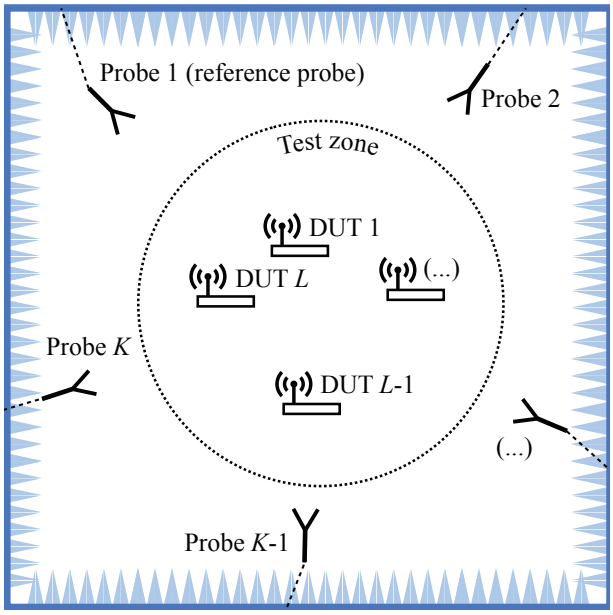

Fig. 2. Example distribution of probe antennas and DUTs in the test zone. They are presumed motionless during test. For demultiplexing, $K > L$.

of the networking stack. A high-level network performance measurand, or Key Performance Indicator (KPI), is what is observable by the user, often throughput or latency [5]. Research and standardization efforts may lead to shared-spectrum KPI tests that point directly to problems that noticeable to end-users and network operators (perhaps the network is "slow" or "won't connect"), but not diagnostic data to troubleshoot underlying causes. Low-level physical signal measurands related to timing, modulation, or power are the usual way to diagnose problems at the device level. How do we apply these methods to over-the-air spectrum sharing tests if they all summed together when they arrive at our signal analyzer?

We propose in this paper a technique to separate baseband waveforms detected from multiple co-channel DUTs, illustrated in Figs. 1 and 2. We establish a two-parameter matrix model to extrapolate multichannel anechoic interactions across frequency (Section II). We develop a method to estimate these parameters from measured data, and invert the probe matrix over frequency to determine probe weights that demultiplex the DUTs (Section III). Last, we demonstrate application to coexistence work by demultiplexing coexisting LTE and Wi-Fi signals (Section IV).

II. Multichannel System Model

This section defines the physical model and notation that underlie the rest of the paper. We reduce the interactions between each probe-DUT pair across a band of interest to a propagation delay and a complex response coefficient.

The environment is an anechoic chamber like the one illustrated in Fig. 2. There are K probe antennas, each connected to a separate channel of a coherent measurement receiver. The receiver acquires complex in-phase and quadrature (IQ) baseband waveforms on all of K channels simultaneously. The test zone in the center of the chamber has $L < K$ DUT transmitters that, during tests, may potentially all transmit simultaneously at the same frequencies.

A. CW Signaling Case - Arbitrary Scattering Environment

First consider an unknown quiet scattering environment. For this subsection only, assume the lth DUT radiates continuous-wave (CW) with magnitude and phase represented voltage phasor V_l^{DUT}. The wave propagates to each of the K receive ports, scaled by transmit-to-receive (DUT-to-probe) response coefficient h_{kl}. The transmit-receive transfer function encapsulates all linear single-frequency attenuation and phase shift: propagation, scattering, impedance mismatch, antenna transduction, receiver frequency response, etc. The component of the voltage phasor received at the k^{th} probe from lth DUT is represented by the phasor V_{kl}. The wave undergoes linear and time-invariant propagation with added receive channel noise, N_k:

$$V_{kl} = h_{kl} V_l^{\text{DUT}} + N_k. \tag{1}$$

We need an equation in terms of probe (not DUT) voltages for over the air (OTA) tests. To this end, define the receive transfer function as relative to a reference probe defined at $k = 1$: $V_{1l} = h_{1l} V_l^{\text{DUT}}$. Solve for V_l^{DUT} and substitute into (1) to find

$$V_{kl} = \frac{h_{kl}}{h_{1l}} V_{1l} + N_k = H_{kl} V_{1l} + N_k. \tag{2}$$

The response coefficient $H_{kl} = h_{kl}/h_{1l}$ for $h_{1l} \neq 0$ relates received phasors, independent of the magnitude or phase of the transmitter. It is no longer strictly a transfer function, because it only relates received signals.

Now let all transmit devices excite CW at the same frequency. Each receive channel is related to the reference receive channel by weighted superposition of each reference antenna transmitter component l:

$$V_k = \sum_{l=1}^{L} H_{kl} V_{1l} + N_k. \tag{3}$$

This is equivalent to matrix multiplication,

$$\mathbf{V} = \mathbf{H}\mathbf{V}_1 + \mathbf{N}. \tag{4}$$

Here $\mathbf{V}$ is the $1 \times K$ row vector of probe receive phasors V_k; $\mathbf{H}$ is the $K \times L$ probe response matrix with elements H_{kl}; $\mathbf{V}_1$ is the $1 \times L$ row vector comprising the demultiplexed voltages at the reference probe, V_{1l}; and $\mathbf{N}$ is the $1 \times K$ row vector of independent and identically distributed (i.i.d.) receive channel noise samples N_k.

The phasor could be normalized as a node voltage in simulation or microwave parameter system like pseudowaves for measurement [6]. The choice of pseudowaves leads to response functions that are a subset of $(K + L)$-port scattering parameters.

B. Modulated Case - Free Field Environment

Each DUT is a communication device, not a swept-frequency CW test instrument; we need to model the channel response for modulated signals. The model will stay tractable in our test scope by exploiting the free-field propagation approximated by the anechoic chamber.

The ideal transmit-receive response in the the $(k,l)^{\text{th}}$ pair in free space is [7]

$$h_{kl}(\omega) = \frac{1}{r_{kl}} \frac{K_k}{\text{AF}_{kl}^{\text{DUT}} \text{AF}_{kl}} e^{jk_0 r_{kl}}. \tag{5}$$

The variables are $\text{AF}_{kl}^{\text{DUT}}$, the complex-valued [8] antenna factor of the DUT antenna l toward the receive antenna k; AF_{kl}, the complex-valued antenna factor of the receive antenna k toward the transmit antenna l; r_{kl}, the separation distance between the $(k,l)^{\text{th}}$ probe-DUT pair; K_k, a calibration factor encapsulating physical constants and corrections for hardware losses and receiver equalization in the receive path of the k^{th} probe; and $k_0 = 2\pi/\lambda_0$, the free-space wavenumber.

The receive impulse response between the k^{th} probe and the 1^{st} probe, with the TEM phase relation $\omega\tau_{kl} = k_0 r_{kl}$, is

$$\begin{aligned} H_{kl}(\omega) &= \frac{h_{kl}(\omega)}{h_{1l}(\omega)} = \frac{\tau_{1l}}{\tau_{kl}} \frac{K_k}{K_1} \frac{\text{AF}_{1l}^{\text{DUT}}}{\text{AF}_{kl}^{\text{DUT}}} \frac{\text{AF}_{1l}}{\text{AF}_{kl}} e^{j\omega(\tau_{kl}-\tau_{1l})} \\ &\approx \overline{H}_{kl} e^{j\omega\Delta\tau_{kl}}. \end{aligned} \tag{6}$$

The complex transfer coefficient $\overline{H}_{kl}$ encapsulates all of the τ, K, and AF terms, which we assume to be frequency-invariant. Each $(k,l)^{\text{th}}$ probe-DUT response is therefore assumed to be a delay $\Delta\tau_{kl}$ in addition to the complex response coefficient $\overline{H}_{kl}$. These two parameters are also the basis of delay-and-sum beamforming [9], though we use it in this paper to excite a mode in the center of the test zone, not form a beam.

The response $H_{kl}(\omega)$ still fits nicely into a matrix equation. The dependence on frequency means (4) now has to be evaluated at each frequency:

$$\mathbf{V}(\omega) = \mathbf{H}(\omega)\mathbf{V}_1(\omega) + \mathbf{N}(\omega). \tag{7}$$

Moving forward, practical use of this expression will depend on determining the delays and response coefficients that characterize $H(\omega)$.

If a calibrated reference probe is available, we can similarly demultiplex the incident co-polarized electric field over frequency, $E_{1l}(\omega)$. The complex antenna factor needs to be known the direction toward each DUT, AF_{1l}, with any necessary impedance and level adjustments K_1:

$$E_{1l}(\omega) = K_1 \text{AF}_{1l}(\omega) V_{1l}(\omega). \tag{8}$$

C. Error Sources

The two-parameter delay and weight model in (6) and (7) requires that a $\Delta\tau_{kl}$ exists that leaves $\overline{H}_{kl}$ invariant across the detection bandwidth. This requires ideal reflectionless transverse electromagnetic (TEM) propagation like the ideal free field.

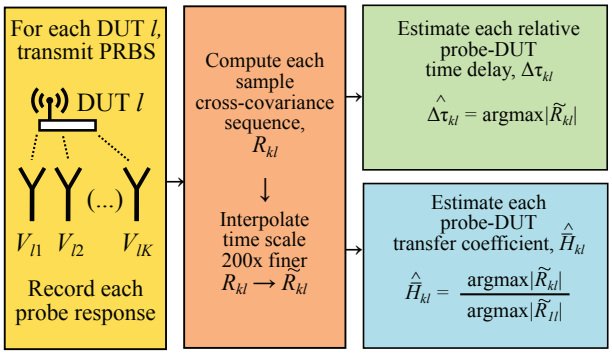

Fig. 3. Summary of the transfer matrix estimation process.

An anechoic chamber approximates this behavior, but other effects arise as error sources, including 1) Reflection interactions in the test zone, 2) Non-TEM near-field interactions for small r_{kl}/k_0, or 3) frequency variation in the ratios $\text{AF}_{kl}^{\text{DUT}}/\text{AF}_{1l}^{\text{DUT}}$, $\text{AF}_{kl}/\text{AF}_{1l}$, and K_k/K_1. The principal impact of these errors on our demultiplexing process is distorted crosstalk between output channels.

III. Probe Weighting

This section details detection and least-squares weighting estimation that we use to demonstrate implementing demultiplexing in this paper. The process is summarized in Fig. 3.

A. Acquiring Alignment Waveforms

All receive channels acquire and store a detection trace composed of M samples of complex IQ baseband voltage at sampling period T_s. Samples are time-synchronized and phase-locked. Sample acquisition occurs at $t[m] = mT_s$ for each $V_{kl}[m]$.

The procedure for collecting channel response calibration data is as follows. At each DUT for $l = \{1, 2, ..., L\}$,

1) Disable all DUTs.
2) Transmit a pseudo-random bit sequence from the l^{th} DUT
3) Simultaneously acquire the receive waveform on all receive channels, $V_{1l}[m], V_{2l}[m], \ldots, V_{Kl}[m]$.

The process results in one M-sample trace for every transmit-receive pair. The $V_{kl}[m]$ are the complete set of calibration data.

B. Probe Response Alignment

We need to estimate $\hat{\overline{H}}_{kl}$ and $\hat{\Delta\tau}_{kl}$ from the alignment data, which we will use to extrapolate the transfer matrix $\mathbf{H}$. The process proposed here was developed intuitively, and is therefore almost certainly suboptimal. Significant improvement may be achieved in further efforts in the future.

The sample cross-correlation sequence $R_{kl}[m]$ between the k^{th} and 1^{st} probe channels excited by the l^{th} DUT iswith respect to the reference antenna is

$$R_{kl}[n] = \sum_{m=1}^{M} (V_{1l}[m]^*) V_{kl}[m+n] \tag{9}$$

$$= \mathcal{F}^{-1}\left\{\mathcal{F}\left(V_{k1}[m]\right)^* \mathcal{F}\left(V_{kl}[m]\right)\right\}. \tag{10}$$

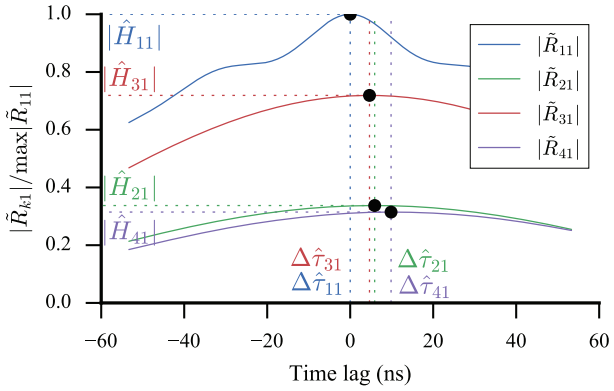

Fig. 4. Example probe channel parameter estimation values taken for DUT 1 (the Wi-Fi AP) from the interpolated cross-correlation sequence $\tilde{R}_{k1}$.

where $\mathcal{F}\{\cdot\}$ denotes discrete Fourier transform and indices n correspond with time lag $\tau[n]$.

The peak of $|R_{kl}[n]|$ is located near the delay we wish to estimate, $\Delta\tau_{kl}$. Digitization results in a quantization error bounded by $\epsilon_\tau = \pm T_s$, resulting in a frequency-domain phase progression error $\Delta\phi$. The worst case is $|\Delta\phi| = 180°$ at the acquisition band edges. To mitigate this we upsample $R_{kl}[n]$ to produce an oversampled $\tilde{R}_{kl}[n]$ on a new time grid $\tilde{\tau}[n] = T_i/T_s\tau[n]$. If $R_{kl}[n]$ has even symmetry about its peak (as under the idealized conditions of Section II), upsampling reduces the maximum phase error to $|\Delta\phi| = (T_i/T_s) \times 180°$. We fix the oversampling factor to $T_i/T_s = 1/1000$ in this work to keep $|\Delta\phi|$ well below 1° across the band.

Each delay pair is estimated by the correlation peak,

$$\Delta\hat{\tau}_{kl} = \underset{\tilde{\tau}}{\operatorname{argmax}} \left|\tilde{R}_{kl}[n]\right|. \tag{11}$$

This is the discrete naïve cross-correlation method of [10] (sampling period T_i). Further robustness to noise may be realized in the future by implementing the complete cross-correlation method from the same source.

We estimate the weight parameter at the corresponding magnitude peaks:

$$\hat{\overline{H}}_{kl} = \frac{\tilde{R}_{kl}\left[\underset{n}{\operatorname{argmax}}\left|\tilde{R}_{kl}[n]\right|\right]}{\tilde{R}_{1l}\left[\underset{n}{\operatorname{argmax}}\left|\tilde{R}_{1l}[n]\right|\right]}. \tag{12}$$

Figure 4 demonstrates the process with data from Section IV.

C. Demultiplexing to Separate DUTs

Now let all DUTs transmit to begin testing. Each measurement receiver channel acquires M_{test} samples. Each transfer function estimator behaves as

$$\hat{H}_{kl}(\omega_n) = \hat{\overline{H}}_{kl} \exp(-j\omega_n \hat{\Delta\tau}_{kl}). \tag{13}$$

The sampling rate can be different from that used to estimate the delay and weighting coefficients in (11)-(12).

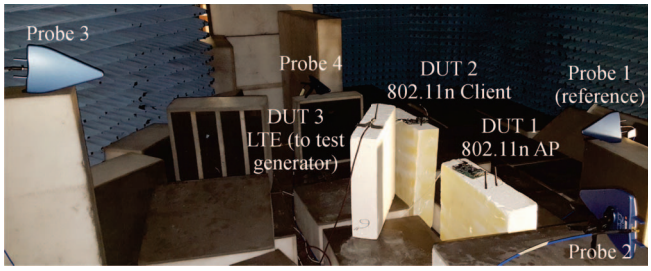

Fig. 5. Our demonstration test used $K = 4$ probes (connected to a 4-channel vector signal transceiver) to demultiplex $L = 3$ DUTs: a pair of Wi-Fi devices and a signal generator sending PRBS LTE.

TABLE I
DUT PARAMETERS

DUTs 1 and 2 (Wi-Fi)		
Protocol standard	802.11n	
Channel center frequency	2.442	GHz
Channel bandwidth	20	MHz
Transmit power setting	20 dBm	
Antenna type	3 cm monopole	
Transport	UDP	
Maximum transport unit	1500	bits
Data payload	Unknown	
DUT 3 (LTE Downlink Generator)		
Protocol standard	LTE FDD	
Center frequency	2.453	GHz
Bandwidth	20	MHz
Modulation type	64QAM	
Transmit power setting	19	dBm
Antenna type	3 cm monopole	
Data payload	PRBS	

The probe weighting matrix from (7) is related to the probe response matrix by inverse:

$$\begin{aligned}\hat{\mathbf{V}}_1(\omega_n) &= \hat{\mathbf{H}}^+(\omega_n)\mathbf{V}(\omega_n) \\ &= \hat{\mathbf{W}}(\omega_n)\mathbf{V}(\omega_n),\end{aligned} \tag{14}$$

where $(\cdot)^+(\omega_n)$ is matrix pseudo-inverse [11] computed at each ω_n. Since each H_{kl} is normalized to h_{1l}, each $\hat{H}_{1l} = 1$, and there is no information in the first row of $\overline{\mathbf{H}}$. Therefore, $\overline{H}_{1l} = 1$ has rank $K - 1$, and $K \geq L + 1$ receive channels are necessary to demultiplex L transmitters.

The time domain baseband can be recovered by IFFT for each row of $\hat{\mathbf{V}}_1(\omega_n)$.

IV. Application to a Coexistence Test

We demonstrate here the results of an initial experiment with this technique applied to LTE and Wi-Fi coexistence.

A. Test Setup

Figure 5 shows the semi-anechoic chamber configured for a Wi-Fi and long-term evolution (LTE) coexistence test.

Like Fig. 2, the DUTs are near the center of the chamber, and the probes are located around the perimeter. This topology provides line-of-sight between each pair of DUTs and maintains the standard practice of the test zone at the center of the chamber for the DUTs [12]. Separation between DUTs

TABLE II
DETECTION SYSTEM PARAMETERS

Probes 1-4		
Antenna type	LPDA	
Manufacturer-specified antenna factor	$\lvert AF_{kl}\rvert = 46$	m^{-1}
2:1 VSWR bandwidth	$600 < f < 6000$	MHz
Acqusition		
Number of channels	4	
Center frequency	$f_c = 2.45$	GHz
Sampling rate	$1/T_s = 60$	MHz
Acquisition count	$M = 10^6$	
Sample size	32	bits
Cross-correlation interpolation factor	$T_s/T_i = 1000$	

is approximately 1 m, and each probe is approximately 1.5 m from the nearest DUT. The short $D = 3$ cm dipoles make these separations much greater than $2D^2/\lambda$.'

Detailed DUT and probe system parameters are in Tables I-II. The probe antennas are all the same make and model of log-periodic dipole antenna (LPDA). Their manufacturer specifies 5 dBi of gain at boresight and linear polarization. Each is oriented to include all DUTs within $\pm 45°$ of boresight at approximately vertical polarization (co-polarized with the DUTs).

Each Wi-Fi DUT is commercial development board hardware with the same make and model. One is configured as an 802.11n access point (AP), and the other is an 802.11n client. A software interface running on a laptop outside the chamber controls the devices during test. We use a bandwidth test mode to radiate by generating uplink (client-to-AP) or downlink (AP-to-client) traffic. These are actual 802.11n devices that use clear channel assessment to sense spectrum; at this close range we expect they will reliably wait to transmit until LTE vacates the channel.

A commercial radio frequency (RF) signal generator instrument excites a carrier modulated with LTE. The modulation data load is PRBS traffic on 10 resource blocks. We pulse the LTE signal at 10 ms period at 50% duty cycle to leave vacant time on the channel for the Wi-Fi system. The signal generator synthesizes the LTE without feedback from the channel, so only the Wi-Fi devices have the sensing information for opportunistic channel use in this test.

B. Calibration Self-Validation

We implemented the probe response alignment described in Section III, and applied the demultiplexing procedure to the original alignment data (baseband traces for each of the 3 DUTs radiating alone). This serves as a validation step, checking that power is dominated by the diagonal terms.

The results are in Fig. 6. Ideally, each l^{th} DUT waveform would appear only at the l^{th} demultiplexer output, and only noise at the other outputs. The crosstalk level averages 21 dB below the desired signal in its column. This figure of merit is the isolation, and needs to be high enough to help a measurement instrument or post-processing tool decode the information transmit by each DUT. The isolation contributes to the dynamic range of demultiplexed detection.

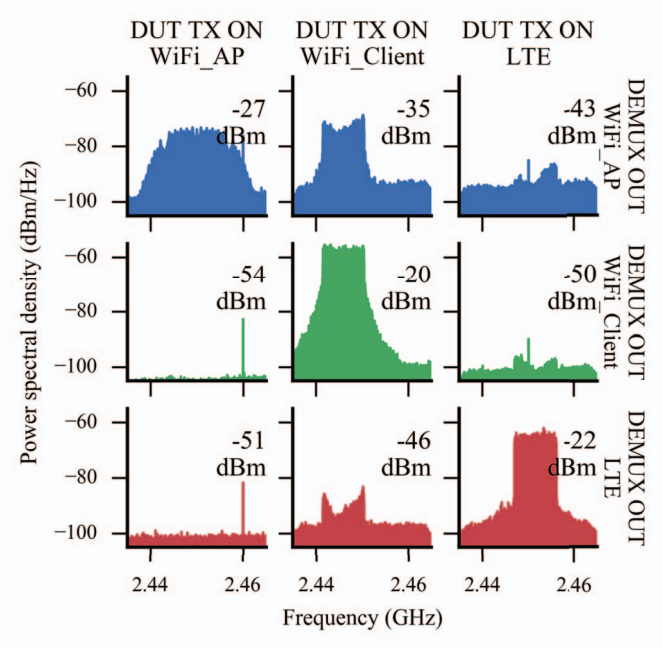

Fig. 6. Demultiplexed and residual cross-talk spectra, shown with total channel power. The average cross-talk level is 21 dB below the desired "through" channel (the diagonal plots in the grid).

TABLE III
CHANNEL UTILIZATION RATES DECOMPOSED BY DUT

	Wi-Fi AP	Wi-Fi Client	LTE	Empty
802.11n downlink test	31%	3%	50%	16%
802.11n uplink test	4%	30%	50%	16%

C. Device-by-Device Channel Occupancy Tests

One use of the demultiplexed output in this application is to study the channel utilization by each DUT jointly over time (during simultaneous co-channel operation). We ran two scenarios to demonstrate this idea, shown in the power envelopes of Fig. 7: a Wi-Fi uplink test with LTE interference, and a Wi-Fi downlink test with LTE interference. For clarity, power levels are averaged in 100 µs bins. Each set of plots shows the three DUT output channels, plus the "no demux" raw data received at the reference antenna for comparison. We emphasize that no spectral filtering or time gating has been applied here to separate the channels.

The principal remaining uncertainty for estimating channel occupancy here is whether a waveform feature is produced by cross-talk the indicated DUT. Figure 6 suggests that the strongest residual cross-talk will be from the Wi-Fi AP channel to the Wi-Fi Client channel. This holds true in both scenarios of Fig. 7. Therefore, assuming that each DUT power envelope at this time-scale is fully "on" or "off," we can define an occupancy power threshold above the cross-talk level for each channel. Moving one-by-one by output channel, we can decompose total channel occupancy by device, even during co-channel transmission. These data are shown in Table III (averaged over one 10 ms on-off period that we applied to the

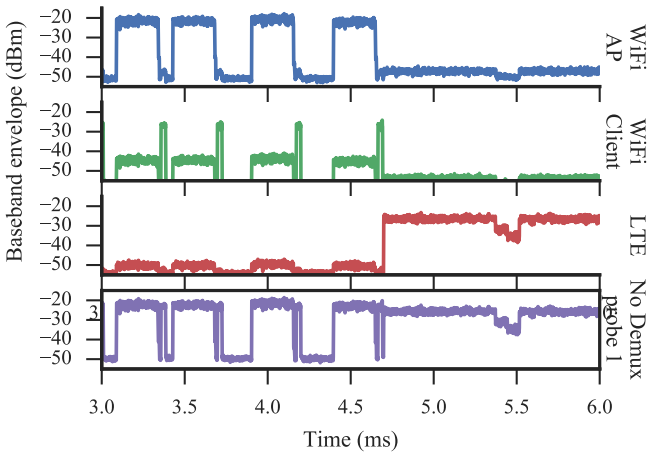

(a) 802.11n downlink test with LTE downlink interference

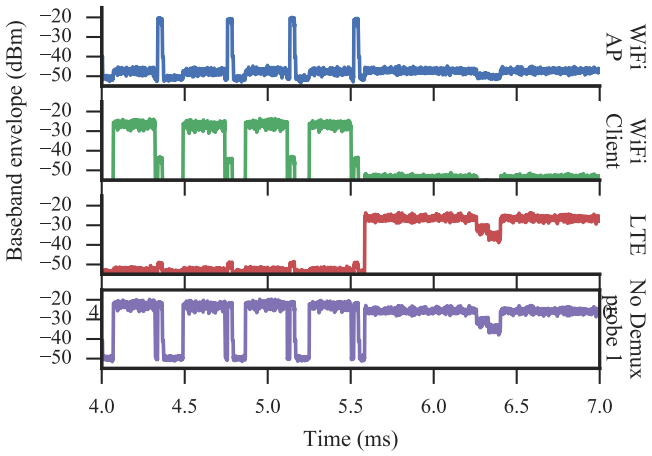

(b) 802.11n uplink test with LTE downlink interference

Fig. 7. The demultiplexed signal envelopes of multiple spectrum-sharing DUTs in two spectrum-sharing coexistence test scenarios. Spatial demultiplexing divided the raw probe data (violet) into separate channels (red, green blue), the waveform components detected from each DUT.

LTE). In each case, the Wi-Fi sender channel occupancy is about 30%, in contrast with the receiving device at 3% to 4%. The LTE generator occupies the channel at a fixed 50% rate as configured on the instrument.

Channel occupancy for multiple co-channel DUTs demonstrated here could be difficult to determine (or define) from test data without demultiplexing. Are the dips in the raw data near 5.5 ms an instance of destructive interference from a collision event, or a feature of a single DUT? Answering this question would need *a priori* information about the constituent signals. However, the demultiplexed outputs show straightforwardly that the dip is a feature of the LTE waveform.

V. Conclusion

We demonstrated spatial demultiplexing of co-channel radiators for testing spectrum sharing and wireless coexistence. The implementation is a simple multiple-input multiple-output (MIMO) receiver. More study will be needed to characterize the processing impacts on the fidelity of the demultiplexed receive channels. Modulation and protocol analysis software may then be able to decode the waveforms for protocol-level insights into a spectrum-sharing scenario.

The data here was post-processed in the frequency domain. However, similar performance might be realized in real-time digital signal processing by developing of a suitable fractional delay filter. The demultiplexing technique could then be integrated aboard a multi-channel detection instrument by including "calibration" or "alignment" feature determine probe weightings. The most challenging practical aspect here may be controlling the DUTs to obtain a channel alignment signal; consumer devices are typically designed to transmit only as part of bi-directional communication with a larger network.

We were careful here to discuss the process and results in terms of detection. Developing this technique into a proper measurement tool will require significant effort in uncertainty analysis for each demultiplexer output channel. This will require characterizing and propagating uncertainty arising from sources such as reflections in the test zone, detector nonlinearity, and antenna responses that do not fit the time delay and coefficient model.

Acknowledgments

The authors are grateful for the valuable ideas and feedback provided by Paul Hale and Peter Jeavons (also with NIST).

References

[1] T. Wheeler, M. Clyburn, J. Rosenworcel, A. Pai, and M. O'Rielly, "Further Notice of Proposed Rulemaking," U.S. Federal Communications Commission, Washington, D.C., Tech. Rep. 15-47, 2015.

[2] "IEEE 802 LAN/MAN Standards Committee 802.22 WG on WRANs (Wireless Regional Area Networks)," Institute of Electrical and Electronics Engineers, New York, NY, Tech. Rep. 802.22.1, 2011.

[3] "Third Memorandum Order and Opinion," Federal Communications Commission, Washington, D.C., Tech. Rep. 12-36, 2012.

[4] M. M. Sohul, M. Yao, T. Yang, and J. H. Reed, "Spectrum Access System for the Citizen Broadband Radio Service," *IEEE Commun. Mag.*, no. 7, pp. 18–25, 2015.

[5] "Key Performance Indicators (KPI) for the Evolved Packet Core (EPC) v. 11," European Telecommunication Standards Institute, Valbonne, FR, Tech. Rep. TS 132 455, 2012.

[6] D. Williams, "Traveling waves and power waves: Building a solid foundation for microwave circuit theory," *IEEE Microw. Mag.*, vol. 14, no. 11, pp. 38–45, 2013.

[7] A. A. Smith, R. F. German, and J. B. Pate, "Calculation of Site Attenuation From Antenna Factors." *IEEE Trans. Electromagn. Compat.*, vol. EMC-24, no. 3, pp. 301–316, 1982.

[8] S. Ishigami, H. Iida, and T. Iwasaki, "Measurements of complex antenna factor by the near-field 3-antenna method," *IEEE Trans. Electromagn. Compat.*, vol. 38, no. 3, pp. 424–432, 1996.

[9] D. Johnson, *Array Signal Processing*. Upper Saddle River, NJ: Prentice-Hall, 1993.

[10] K. Coakley and P. Hale, "Alignment of noisy signals," *IEEE Trans. Instrum. Meas.*, vol. 50, no. 1, pp. 141–149, 2001.

[11] R. Penrose, "A Generalized Inverse for Matrices," *Math. Proc. Cambridge Philos. Soc.*, vol. 51, no. 7, pp. 406–413, 1955.

[12] A. Simmons and W. Emerson, "An Anechoic Chamber Making Use of a New Broadband Absorbing Material," in *IRE Int. Conv. Rec.*, vol. 1, 1958, pp. 34–41.